Lasers in Manufacturing Conference 2019

Optimization of mechanical properties and as-built quality of additive manufactured hypereutectic Al-Si alloys using ultra-short laser pulses

Tobias Ullsperger[a*], Gabor Matthäus[a], Lisa Kaden[a], Brian Seyfarth[a,b], Hannes Engelhardt[c], Dongmei Liu[c], Markus Rettenmayr[c], Stefan Nolte[a,b]

[a]*Institute of Applied Physics, Abbe Center of Photonics, Friedrich-Schiller-Universität Jena, Albert-Einstein-Strasse 15, 07745 Jena, Germany*

[b]*Fraunhofer Institute for Applied Optics and Precision Engineering, Albert-Einstein-Strasse 7, 07745 Jena, Germany*

[c]*Otto Schott Institute of Materials Research, Friedrich-Schiller-Universität Jena, Löbdergraben 32, 07743 Jena, Germany*

Abstract

Rapidly solidified hypereutectic Al-Si alloys are characterized by high tensile strength, hardness and low thermal expansion. For example, by adapting the mass fraction of silicon they are predestined for thermal expansion matched housings and scaffolds. Additive manufacturing with ultra-short laser pulses results in high cooling rates and a highly confined melt pool, which reduces or avoids segregation in the solidified phases. In this talk, powder bed fusion of Al-Si with silicon contents of more than 20wt% using 500fs laser pulses at a wavelength of 1030nm is presented. The resulting microstructure differs significantly from that in casting or conventional powder bed methods, revealing a fine distribution of sub-micron sized primary silicon particles. Moreover, the underlying laser scanning strategy has a crucial impact on the as-built quality including surface roughness, density and hardness. We demonstrate, that Al-Si alloys with extremely high silicon contents up to 70wt% can be harnessed for additive manufacturing applications.

Keywords: Additive manufacturing; Laser powder bed fusion; Selective laser melting; SLM; Ultra-short laser pulses; Hypereutectic Al-Si alloys; Light-weight materials.

1. Motivation and state of knowledge

Aluminum silicon (Al-Si) alloys are one of the most important cast alloys for the construction of light-weight components in automotive, shipbuilding, aircraft and aerospace applications [1]. These alloys are distinguished by their high strength over weight ratio, high specific stiffness, excellent castability, wear resistance and low thermal expansion coefficient [1,2], which can be further improved by an increasing

silicon content. The main disadvantage for the broad industrial use of hypereutectic Al-Si alloys with silicon contents of more than 12.6% is the formation of irregular, coarse and brittle primary silicon particles and plates due to the low cooling rates by using conventional casting techniques [3-7], resulting in a degradation of tensile strength and ductility and finally the formation of cracks. For several decades, some physical methods have been exploited to refine the primary silicon phase in pure Al-Si. The most prominent techniques based on melt overheating [8,9], rapid solidification by a large thermal gradient [10], high undercooling of the liquid phase [6,11,12] and electromagnetic stirring [13,14] or any appropriate combination. Some methods, like spray forming [7], melt spinning [10,15,16] and container-less solidification by electromagnetic levitation [17] enable an effective refinement, but they include complicated processing environments, expensive equipment and in particular the geometrical variety of the manufactured samples is severely limited.

In contrast, laser metal fusion offers new possibilities to fabricate near net shape components with minimum post-processing efforts. Micro cladding [12,18-20] and laser metal fusion (LMF) [21] with continuous wave lasers have shown, that primary silicon can be refined up to 40% of silicon as a result of high cooling rates in the range of 10^3-10^8 K/s [22-25]. Nevertheless, a refinement at significantly higher silicon contents has not yet been demonstrated with these techniques and the precision of manufactured structures are limited by the extensive melt pool in the range of several hundreds of micrometers in each dimension.

In this work, we are using ultra-short laser pulses to selectively fuse pre-alloyed Al-Si grains containing silicon of up to 70%. Previous investigations have shown that a controlled heat accumulation [26,27] combined with a high peak power induced by short laser pulses in the sub-picosecond range are beneficial to melt powder materials with a high melting point as well as a high reflectivity, such as tungsten and pure copper [28-32]. The reduced heat affected zone leads to a confined melt pool and therefore structure sizes below 100µm. Furthermore the influence of the laser parameters on the size and distribution of primary silicon in hypereutectic Al-Si alloys could be demonstrated [33].

In the present study we focus on the additive manufacturing of extreme hypereutectic Al-Si alloys and the effects of the pulsed laser interaction on the microstructure. Furthermore advanced scanning methods are developed and investigated to improve the as-built quality of the manufactured samples.

2. Experimental setup and methodology

In our experiments we are using a home-made fully automated laser metal fusion setup, which is shown in Fig. 1. Powder is distributed layer-wise by a moving re-coater that spreads the powder from an upward-moving powder supplier stage on the built-platform. Subsequently a galvano-scanner (IntelliScan by *Scanlab*) deflects the laser beam over the powder surface and the grains fused to the desired pattern. Afterwards the built-platform is moved downwards by a defined layer-thickness and the process starts again. Layer-by-layer a solid part is fabricated inside the powder bed. During the process the chamber is flooded by nitrogen to avoid oxidation and the smoke is exhausted by a rotary vane pump.

The ultra-short pulse laser system (*Active Fiber Systems*) delivers pulses with a duration of 500fs at a wavelength of 1030nm. The maximum applicable average output power on the surface of the powder bed is 25W at a repetition rate of 20MHz. The pulses are focused with a 160mm F-theta lens resulting in a $1/e^2$ spot diameter of 50µm. For the sake of enhanced comparability the wavelength of the laser as well as the focusing conditions in these experiments are almost similar to the settings in conventional LSM-machines.

The powder material is produced by gas atomization of an Al-Si melt and was provided by *Nanoval and TLS-Technik*. The sphere-like grains have a size distribution of 20-63µm with an average diameter of 38µm.

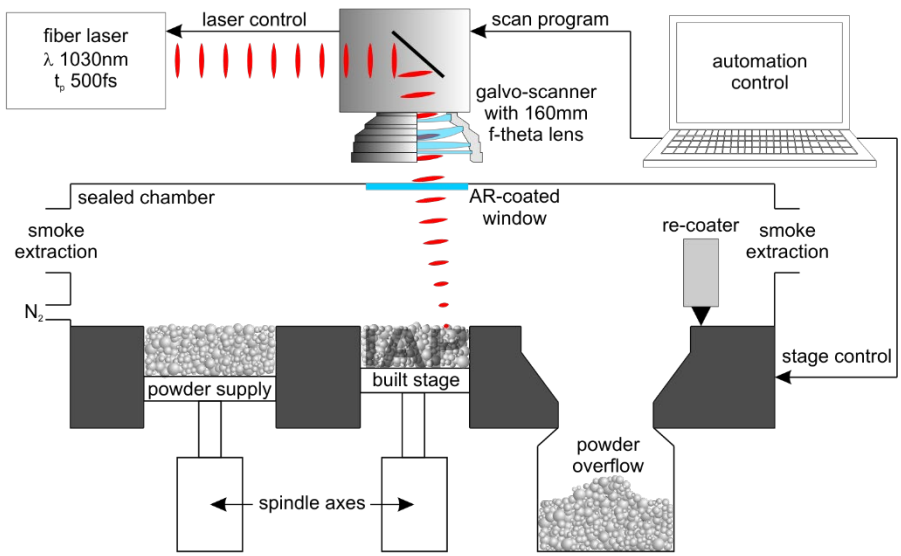

Fig. 1. Scheme of the fully automated laser-fusion setup combined with a femtosecond fiber laser system.

The fabricated samples are analyzed by scanning electron microscopy (SEM) and laser scanning microscopy (LSM) to qualify solidification characteristics as well as surface topography. Additionally the samples are embedded in epoxy resin and polished with an Al_2O_3 suspension to reveal the separated phases of Al-Si and are visualized with a light microscope. The effect of the scanning strategies on the microstructure and the local mechanical properties are substantiated by measuring the Brinell hardness.

In the experiments the pulse energy (E_p) and scanning speed (v_{scan}) are variied while the repetition rate (f_{rep}), the spot diameter on the surface of the powder bed (d_S), the wavelength and the pulse duration are fixed to 20MHz, 50µm, 1030nm and 500fs, respectively. In order to compare the effects of the different power levels, the total amount of energy concerning a specific track length, the so called *energy per unit length* is used. It combines the average power (P_{av}) with the scan speed:

$$Q = \frac{E_p \cdot f_{rep}}{v_{scan}} = \frac{P_{av}}{v_{scan}} \qquad (1)$$

3. Experimental setup and methodology

In previous studies the optimized processing regime for additive manufacturing of single walled structures in Al-Si40 with 500fs pulses at 20MHz was determined [33]. At an average power of 25W and a scan speed of 200mm/s (Q = 125J/m) the most homogeneously molten structures were obtained.

3.1. Laser and scanning parameters

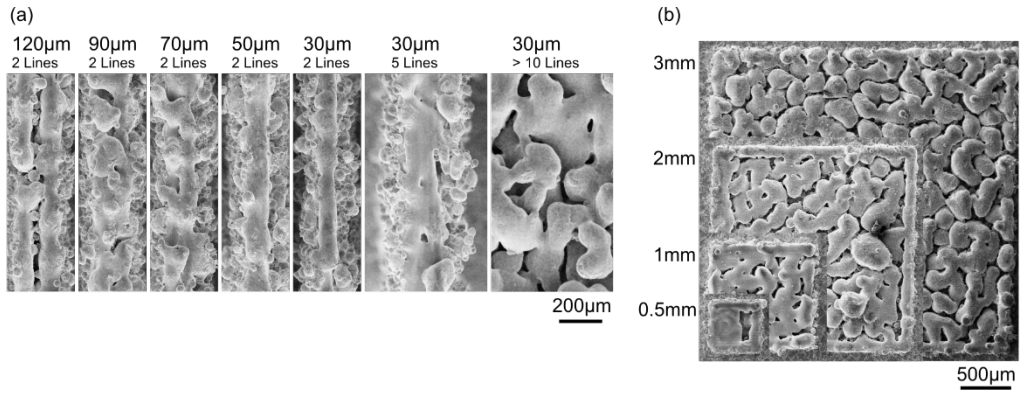

Fig. 2. SEM-images of two adjacent molten tracks with decreasing hatch spacing at 25W and 200mm/s (a). The two images at the right show the solidification behavior with 5 and more than 10 neighboring hatch lines. The compilation in (b) compares the influence of the island size on the solidification.

Object of the following investigations is the solidification behavior by melting large areas of Al-Si40 with these parameters. In Fig. 2 (a) SEM images of two solidified adjacent scanned lines (10mm) with decreasing hatch spacing are shown. The layer thickness is 25µm and the generated walls were built up to a total height of 5mm. Due to the melt width of 90µm two separated lines with a gap in-between can be seen at a spacing of 120µm. Further reduction of the distance leads to a fusion of both tracks. Between 70-90µm the molten surface shows an instable melt with various interruptions. At around 60µm and below it turns into a homogeneous solidification. This behavior can also be observed by connecting up to 10 neighboring tracks (see 30µm, 5 in Fig. 2 (a)). At a larger number of tracks as can be seen on the last image on the right of Fig. 2 (a), the surface is getting rough again with numerous unwanted inclusions that reduces the density of the fabricated part. This behavior can be explained by the fact, that the first molten track is almost cooled down when the second track is scanned. The melting front tries to merge to the subsequent solidified structures and due to the low thermal penetration and poor wettability an instable melt occurs. Additionally the strong local melting due to the high intensive pulses leads to an extensive growth of the track in vertical direction. Hence, a lateral shrinkage of the powder bed could be observed, so that less powder grains are present for the next track.

In Fig. 2 (b) the size of the area, so-called islands was varied. The hatch spacing was 30µm and the layer thickness 25µm. It can be seen, that a low scan length of 0.5mm is short enough to maintain a hot stable melt which results into a flat and homogeneous surface. With increasing island size the surface roughness and imperfections are increasing as well.

3.2. Optimization of as-built roughness

In laser metal fusion the scan strategy has crucial influence on the density, mechanical properties, the thermally induced stress and the roughness of the final part [34]. With reference to the results in the previous section, systematic investigation of the scan strategy to improve the solidification characteristic and as-built surface roughness have been carried out. In Fig. 3 the average roughness in relation to the used scan strategy is shown. The average power of 25W and scan speed of 200mm/s is constant for all samples with an edge length of 2mm and height of 1mm. The basic layer thickness is 30µm, whereas N indicates the number of sublayers. The first scan strategy contains a simple line-by-line pattern, which was also used in section 3.1.

Every single line is scanned in the same direction next to the other with a hatch distance of 30µm. The average roughness is 19µm. The first approach to improve the roughness was to divide the area into islands with a slight overlap of 50µm. At a size of 0.5 x 0.5mm^2 the roughness could be significantly reduced to 6µm.

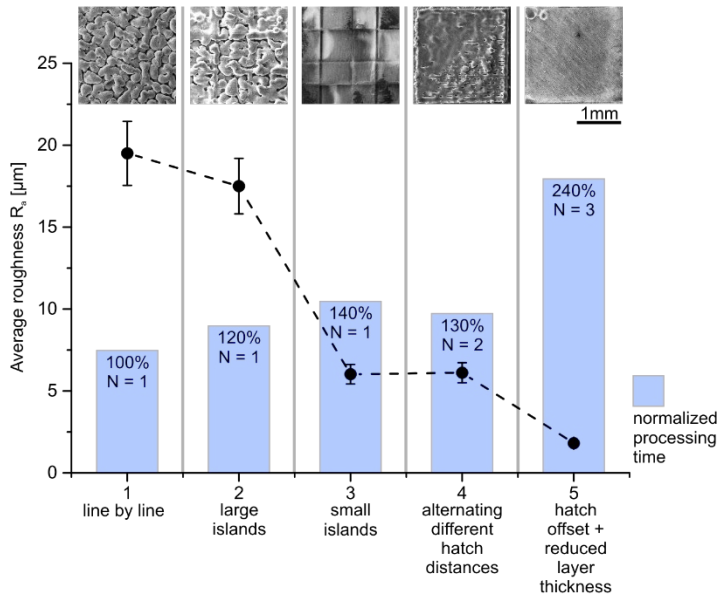

Fig. 3. Overview of the measured roughness depending on the scan strategy. N denotes the number of sublayers for with regards to a layer thickness of 30µm.

Another strategy to avoid a complex division into islands is the laser metal fusion in two stages (4). At first a powder layer with a thickness of 15µm is coated and scanned with a large hatch distance of 100µm. This results in a dense and uniform grid with intended gaps that will be filled with the next 15µm sublayer. This layer is processed with a hatch distance of 30µm under an angle of 45°. Therefore, the gaps are filled will melt and the surface is smoothed leading to a roughness value that is comparable to the island strategy.
A further improvement was achieved by the selective melting in three stages (5). In the first stage the line-by-line pattern has a hatch distance of 150µm at a layer thickness of 15µm. In the second stage a new 15µm powder layer was coated and an offset of the whole line pattern of 75µm was applied to fill the remaining gaps. In the last stage the built platform maintained the previous position and fresh powder was coated and scanned with a hatch distance of 30µm. The resulting smooth surface has a roughness of just 1.6µm but the fabrication time is more than two times as long as for the first reference scan strategy.

3.3. Improvement of mechanical properties

The results of the surface quality indicate that imperfections and inclusions lead to a decrease in the mechanical properties. In Fig. 4 the Brinell hardness and density in dependence on the fabrication method are compiled for Al-Si40. Brinell hardness was determined by pressing a sintered hard metal sphere with a diameter of 2.5mm and a load of 62.5kp (623N) for 20s on the polished surface of the sample (in accordance with ASTM E10; ISO 6506) and measuring the imprint diameter. The calculated hardness value is approximately linearly related to the ultimate tensile strength for low-alloys steels [35] and can be used as a rough estimation of the strength for Al-Si40. The effects of underlying pores and inclusion affects the imprint depth directly and consequently influences the hardness in a negative way.

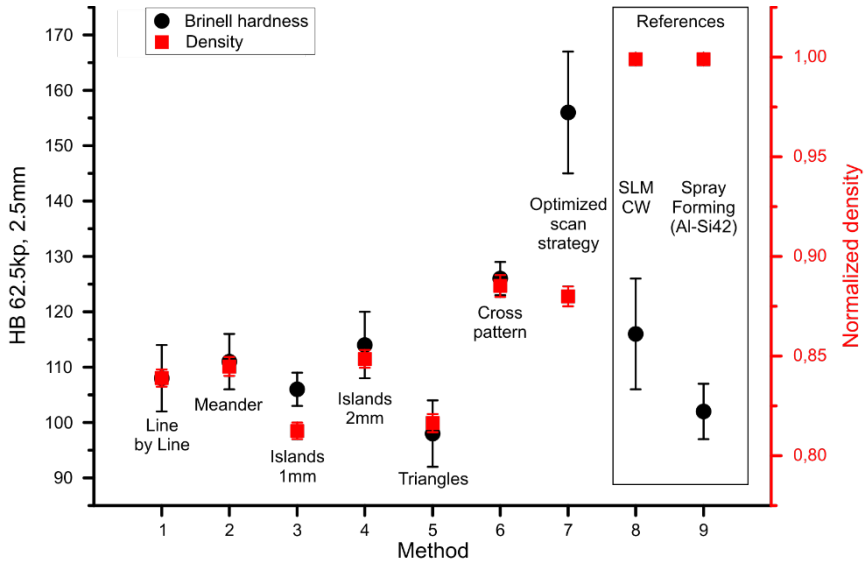

Fig. 4. Compilation of Brinell hardness and relative density (Al-Si40) in dependence on the scan strategy. In comparison two references are shown on the right site. One is produced with a commercial LMF-system and another was fabricated by spray forming spinning (*Osprey Metals Ltd.*).

In addition to the already presented scan strategies further advanced scan patterns were tested. "Meander"-like motion is a line-by-line pattern where the direction of the scanned line is alternating. "Triangles" is an equilateral triangular pattern that is rotated step-wise over the whole area and offers a more uniform thermal distribution during the melting process. "Cross" is a dendritic pattern with an indentation size in the range of the hatch distance. The "optimized scan strategy" is a combination of strategy (4) and (5) referring to Fig. 3. In all cases the layer thickness was decreased to 20µm to improve the vertical connection.

As can be seen in Fig. 4 the density of the fabricated samples in the range of 82% to 89% are roughly related to the hardness, except for the optimized scan strategy. Here, the Brinell hardness is approximately 1.5 times higher than for the other ones. Furthermore this value is much higher than for the reference samples produced with a conventional LMF-system and via spray forming by *Osprey Metals Ltd.* even if the density in this case is close to the ideal value. One important reason is that the silicon phase is more refined and the primary silicon particles are distributed more homogeneously as can be seen in the next chapter.

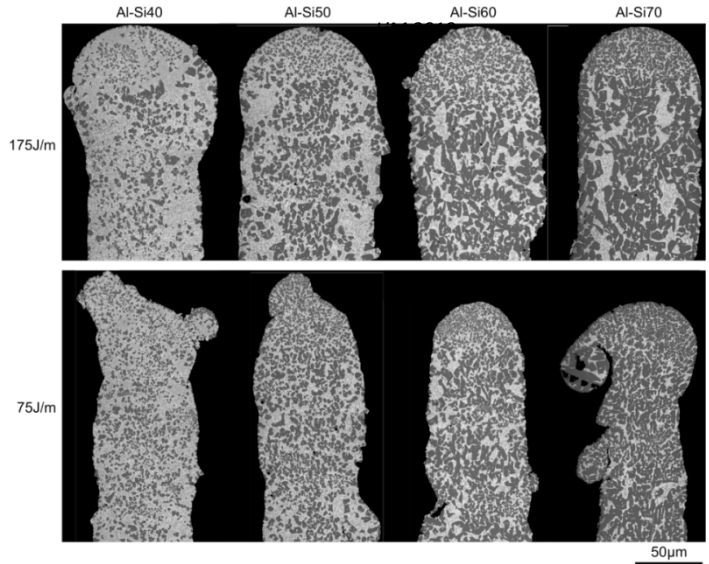

Fig. 5. Polished cross-sections of manufactured single walls with silicon contents of 40, 50, 60 and 70% for 175J/m and 75J/m at 25W and a layer thickness of 10µm.

3.4. Laser metal fusion of extreme hypereutectic Al-Si

The microstructure of hypereutectic Al-Si alloys consists of three phases: α-Al with 1.65% solved Si, eutectic Si and primary silicon. In order to analyze the characteristics of the microstructure of alloys with extreme Si mass contents influenced by the pulsed laser irradiation, single walled structures were fabricated with a layer thickness of 10µm and a constant power of 25W. In Fig. 5 light microscopic images of the microstructures of vertical cross-sections made of Al-Si40,-50,-60 and -70 are shown. Solid fully molten walls could be manufactured that only have a few micron-sized gas pores. The size of the primary silicon particles (dark areas) are steadily increasing with increasing silicon content. At 40% and 50% the polyhedral growth of silicon dominates, which indicates a large undercooling of the melt [4]. Using a high energy per unit length (e.g. 175J/m) an accumulation of particles with growing size could be observed in the center and at the boundaries. This is an effect of the lateral Gaussian intensity distribution of the laser pulses. The thermal gradient is directly related to the gradient of the intensity distribution. Thus, the thermal gradient on the rising and falling edge is much higher than in the center and at the boundaries, resulting in a higher cooling rate. Therefore, a refinement of primary silicon is more pronounced in that region. At a much lower line energy of 75J/m a more uniform distribution and smaller size of primary silicon is observed in all investigated alloys.

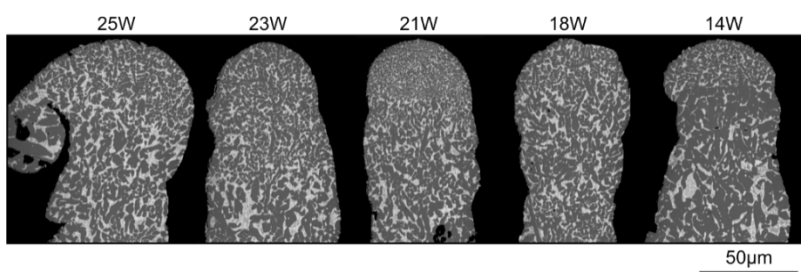

Fig. 6. Polished cross-section of single walls made of Al-Si70 at different average powers and a constant energy per unit length of 75J/m.

In Fig. 6 the microstructures of Al-Si70 at 75J/m for different average powers are presented. The optimum refinement and uniformity of Si particle distribution could be found at 21W. Hence, it is possible to control the growth and nucleation of primary silicon by melting with ultra-short laser pulses in a specific range yielding highly confined, fully molten light weight structures below 100µm even for extreme hypereutectic Al-Si alloys.

4. Summary and Outlook

The results of this work show the potentials and the challenges in ultra-short laser pulse assisted selective melting of hypereutectic Al-Si alloys. The lateral fusion of scanned tracks results in some imperfections on the surface leading to a roughness of nearly 20µm. Advanced scanning strategies were developed and investigated that have finally improved the as-built roughness to less than 5µm.

The maximum achieved density with almost 90% is still far from optimum. Nevertheless the maximum Brinell hardness value could be estimated to 155 (HBW 2.5/62.5kp) which is much larger than the hardness values obtained by samples that have been produced with an optimized parameter setting on a commercial LMF-machine (116 HBW) and in comparison to semi-finished parts produced by spray forming (102 HBW).

Finally we could show that ultra-short laser pulses can be used to fuse Al-Si even with extremely high silicon mass contents of up to 70%. At the same time the control of the reduced heat affected zone in comparison to conventional cw lasers with more than 100W could be utilized to adjust the microstructural features in a defined range.

Acknowledgements

We acknowledge support by the German Federal Ministry of Education and Research (BMBF) within the project AM-OPTIS (02P15B203) and the Deutsche Forschungsgemeinschaft (DFG) within the SPP 2122 MATframe (462/13-1).

References

[1] Ostermann, F., 2014. Anwendungstechnologie Aluminium, Springer-Verlag, Berlin Heidelberg New York.

[2] Olakanmi, E.O., Cochrane, R.F., Dalgarno, K.W., 2015. A review on selective laser sintering/melting (SLS/SLM) of aluminum alloy powders: Processing, microstructure, and properties, Progress in Material Science 74, pp. 401-477.

[3] Robles-Hernandez, F.C., Herrera, R., Jose, M., Mackay, R., 2017. Al-Si Alloys: automotive, aeronautical, and space applications, Springer International Publishing,

[4] Vijeesh, V., Prabhu, K.N., Review of Microstructure Evolution in Hypereutectic Al-Si Alloys and its Effect on Wear Properties, 2015. Transactions of the Indian Institute of Metals 76(1), pp. 1-18.

[5] Zhao, L.Z., Zhao, M.J., Song, L.J., Mazumder, J., 2014. Ultra-fine Al–Si hypereutectic alloy fabricated by direct metal deposition, Materials and Design 56, pp. 542–548.

[6] Jia, Y., Cao, F., Scudino, S., Ma, P., Li, H., Yu, L., Eckert, J., Sun, J., 2014. Microstructure and thermal expansion behavior of spray-deposited Al-50Si, Materials and Design 57, pp. 585–591.

[7] Chien, C.W., Lee, S.L., Lin, J.C., Jahn, M.T., 2002. Effects of Si_P size and volume fraction of Al/Si_P, Materials Letters 52(4), pp. 334–341.

[8] Jung, J.-G., Ahn, T.-Y., Cho, Y.-H., Kim, S.-H., Lee, J.-M., 2018. Synergistic effect of ultrasonics melt treatment and fast cooling on the refinement of primary Si in a hypereutectic Al-Si alloy, Acta Materialia 144, pp. 31–40.

[9] Li, P., Nikitin, V.I., Kandalova, E.G., Nikitin, K.V., 2002. Effect on melt overheating, cooling and solidification rates Al-16wt.%Si alloy structures, Materials Science an Engineering: A 332(1), pp. 371–374.

[10] Xu, C.L., Wang, H.Y., Qiu, F., Yang, Y.F., Jiang, Q.C., 2006. Cooling rate and microstructure of rapidly solidified Al–20wt.% Si alloy, Materials Science and Engineering: A 417(1), pp. 275–280.

[11] Kobayashi, K., Shingu, P.H., H., Kanbara, H., Ozaki, R., 1976. The Role of the Primary Phase on Eutectic Solidification of Al-Si Alloys, Transactions of the Japan Institute of Metals 17, pp. 545–550.
[12] Pei, Y.T., De Hosson, J.T.M., 2000. Functionally graded materials produced by laser, Acta Materialia 48(10), pp. 2617–2624.
[13] Robles-Hernandez, F.C., Sokolowski, J.H., 2006. Comparison among chemical and electromagnetic stirring and vibration melt treatments for Al-Si hypereutectic alloys, Journal of Alloys and Compounds 426(1), pp. 205–212.
[14] Lu, D., Jiang, Y., Guan, G., Zhou, R., Li, Z., Zhou, R., 2007. Refinement of primary Si in hypereutectic Al-Si alloy by electromagnetic stirring, Journal of Materials Processing Technology 189(1), pp. 13–18.
[15] Bendijk, A., Delhez, R., Katgerman, L., De Keijser, T.H., Mittemeijer, E.J., Van Der Pers, N.M., 1980. Characterization of Al-Si-alloys rapidly quenched from the melt, Journal of Materials Science 15(11), pp. 2803-2810.
[16] Xu, C.L., Jiang, Q.C., 2006. Morphologies of primary silicon in hypereutectic Al-Si alloys with melt overheating temperature and cooling rate, Materials Science and Engineering: A 437(2), pp. 451-455.
[17] Liu, R.P., Herlach, D.M., Vandyoussefi, M., Greer, A.L., 2004. Undercooling and Solidification of Al-50 At. Pct Si Alloy by Electromagnetic Levitation, Metallurgical and Materials Transactions A 35(2), pp. 607-612.
[18] Grigoriev, S.N., Tarasova, T.V., Gvozdeva, G.O., Nowotny, S., 2014. Structure Formation of Hypereutectic Al-Si-Alloys Produced by Laser Surface Treatment, Journal of Mechanical Engineering 60(6), pp. 389-394.
[19] Grigoriev, S.N., Tarasova, T.V., Gvozdeva, G.O., Nowotny, S., 2015. Solidification behaviour during laser microcladding of Al-Si alloys, Surface and Coatings Technology 268, pp. 303-309.
[20] Grigoriev, S.N., Tarasova, T.V., Gvozdeva, S., 2016. Optimization of Parameters of Laser Surfacing of Alloys of the Al-Si System, Metal Science and Heat Treatment 57(9), pp. 589-595.
[21] Hilpert E., Risse, S., 2015. Additive manufacturing of aluminum alloy with high silicon content, Materials Science & Technology Conference and Exhibition, MS&T 1, pp. 101-108.
[22] Das, M., Krishna, Balla, V.K., Basu, D., Bose, S., Bandyopadhyay, A., 2010. Laser processing of SiC-particle-reinforced coating on titanium, Scripta Materialia 63(4), pp. 438-441.
[23] Zhong, M., Liu, W., 2010. Laser surface cladding: The state of the art and challenges, Proceedings of the Institution of Mechanical Engineers, Part C: Journal of Mechanical Engineering Science 224(5), pp. 1041-1060.
[24] Hong, C., Gu, D., Dai, D., Cao, S., Alkhayat, M., Jia, Q., Gasser, A., Weisheit, A., Kelbassa, I., Zhong, M., Poprawe, R., 2015. High-temperature oxidation performance and its mechanism of TiC/Inconel 625 composites prepared by laser metal deposition additive manufacturing, Journal of Laser Applications S17005.
[25] Gu, D., Wang, H., Zhang, G., 2014. Selective Laser Melting Additive Manufacturing of Ti-Based Nanocomposites: The Role of Nanopowder, Metallurgical and Materials Transactions A 45(1), pp. 464-476.
[26] Richter, S., Döring, S., Tünnermann, A., Nolte, S., 2011. Bonding of glass with femtosecond laser pulses at high repetition rates, Applied Physics A 103(2), pp. 257-261.
[27] Eaton, S.M., Zhang, H., Herman, P.R., Yoshino, F., Shah, L., Bovatsek, J., Arai, A.Y., 2005. Heat accumulation effects in femtosecond laser-written waveguides with variable repetition rate, Optics Express 13(12), pp. 4708-4716.
[28] Ebert, R., Ullmann, F., Hildebrandt, D., Schille, J., Hartwig, L., Kloetzer, S., Streek, A., Exner, H., 2012. Laser Processing of Tungsten Powder with Femtosecond Laser Radiation, JLMN-Journal of Laser Micro/Nanoengineering Vol. 7(1).
[29] Ebert, R., Ullmann, F., Schille, J., Loeschner, U., Exner, H., 2013. Investigation of cw and ultrashort pulse laser irradiation of powder surfaces – a comparative study, Proceedings of SPIE Vol. 8607, 86070X.
[30] Nie, B., Huang, H., Bai, S., Liu, J., 2015. Femtosecond laser melting and resolidifying of high-temperature powder materials, Applied Physics A 118(1), pp. 37-41.
[31] Nie, B., Yang, L., Huang, H., Bai, S., Wan, P., Liu, J., 2015. Femtosecond laser additive manufacturing of iron and tungsten parts, Applied Physics A 119(3), pp. 1075-1080.
[32] Kaden, L., Matthäus, G., Ullsperger, T., Engelhardt, H., Rettenmayr, M., Tünnermann, A., Nolte, S., 2017. Selective laser melting of copper using ultrashort laser pulses, Applied Physics A, 123 (596).
[33] Ullsperger, T., Matthäus, G., Kaden, L., Engelhardt, H., Rettenmayr, M., Risse, S., Tünnermann, A., Nolte, S., 2017. Selective laser melting of hypereutectic Al-Si40-powder using ultra-short laser pulses, Applied Physics A, 123 (798).
[34] Ali, H., Ghadbeigi H., Mumtaz K., 2018. Effect of scanning strategies on residual stress and mechanical properties of Selective Laser, Materials Science and Engineering: A 712, pp. 175-187.
[35] Pavlina, E.J., Vantyne C., 2008. Correlation of Yield Strength and Tensile Strength with Hardness for Steels, Journal of Materials Engineering and Performance 17(6), pp. 888-893.